J|A|C|S ARTICLES

Published on Web 10/26/2010

Mechanistic Studies of the Oxygen Evolution Reaction by a Cobalt-Phosphate Catalyst at Neutral pH

Yogesh Surendranath, Matthew W. Kanan,† and Daniel G. Nocera*

Department of Chemistry, 6-335, Massachusetts Institute of Technology, Cambridge, Massachusetts 02139-4307, United States

Received July 9, 2010; E-mail: nocera@mit.edu

Abstract: The mechanism of the oxygen evolution reaction (OER) by catalysts prepared by electrodepositions from Co^{2+} solutions in phosphate electrolytes (Co-Pi) was studied at neutral pH by electrokinetic and ^{18}O isotope experiments. Low-potential electrodepositions enabled the controlled preparation of ultrathin Co-Pi catalyst films (<100 nm) that could be studied kinetically in the absence of mass transport and charge transport limitations to the OER. The Co-Pi catalysts exhibit a Tafel slope approximately equal to 2.3 × *RT/F* for the production of oxygen from water in neutral solutions. The electrochemical rate law exhibits an inverse first order dependence on proton activity and a zeroth order dependence on phosphate for [Pi] ≥ 0.03 M. In the absence of phosphate buffer, the Tafel slope is increased ~3-fold and the overall activity is greatly diminished. Together, these electrokinetic studies suggest a mechanism involving a rapid, one electron, one proton equilibrium between Co^{III}−OH and Co^{IV}−O in which a phosphate species is the proton acceptor, followed by a chemical turnover-limiting process involving oxygen−oxygen bond coupling.

Introduction

Solar-driven electrochemical splitting of water to produce hydrogen and oxygen is a high energy density method for the storage of solar energy.[1,2] This solar-to-fuels conversion consists of the four electron, four proton oxidation of water to oxygen and the reduction of the produced protons to hydrogen. Of these two half-reactions, the oxygen evolution reaction (OER) is particularly demanding because it requires the distribution of four redox processes over a narrow potential range, the coupling of multiple proton and electron transfers, and the formation of two oxygen−oxygen bonds.[3−10] The efficiency and conditions required for this reaction are key determinants of the overall viability of energy storage via water-splitting. As such, the continued development of effective OER catalysts and elucidation of their mechanisms stand as central scientific and technological challenges in energy conversion.

Scheme 1

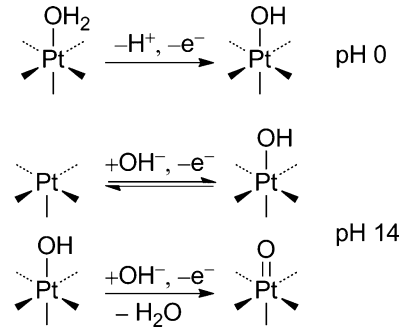

Conductive transition metal oxides have been shown to promote the OER with high efficiency and current density under either highly acidic or highly alkaline conditions.[11−14] There are two basic classes of metal oxide catalysts: those comprising precious metals and those comprising first row transition metals. Extensive mechanistic studies have been performed for the OER catalyzed by platinum oxides. Distinct mechanisms prevail under acidic and alkaline conditions (Scheme 1). The proposed reaction for the OER under acidic conditions entails water binding to the surface and the irreversible removal of one electron and one proton to form a platinum hydroxide.[15−18] In alkaline media, a reversible binding of hydroxide ion coupled to a one electron

† Present address: Department of Chemistry, Stanford University, Stanford, CA 94305-5080.

(1) Nocera, D. G. *Inorg. Chem.* **2009**, *48*, 10001–10017.
(2) Lewis, N. S.; Nocera, D. G. *Proc. Natl. Acad. Sci. U.S.A.* **2006**, *103*, 15729–15735.
(3) Siegbahn, P. E. M. *J. Am. Chem. Soc.* **2009**, *131*, 18238–18239.
(4) Concepcion, J. J.; Jurss, J. W.; Brennaman, M. K.; Hoertz, P. G.; Patrocinio, A. O. T.; Murakami Iha, N. Y.; Templeton, J. L.; Meyer, T. J. *Acc. Chem. Res.* **2009**, *42*, 1954–1965.
(5) Betley, T. A.; Wu, Q.; Van Voorhis, T.; Nocera, D. G. *Inorg. Chem.* **2008**, *47*, 1849–1861.
(6) Betley, T. A.; Surendranath, Y.; Childress, M. V.; Alliger, G. E.; Fu, R.; Cummins, C. C.; Nocera, D. G. *Phil. Trans. Royal Soc. B* **2008**, *363*, 1293–1303.
(7) Huynh, M. H. V.; Meyer, T. J. *Chem. Rev.* **2007**, *107*, 5004–5064.
(8) Dempsey, J. L.; Esswein, A. J.; Manke, D. R.; Rosenthal, J.; Soper, J. D.; Nocera, D. G. *Inorg. Chem.* **2005**, *44*, 6879–6892.
(9) Chang, C. J.; Chang, M. C. Y.; Damrauer, N. H.; Nocera, D. G. *Biophys. Biochim. Acta* **2004**, *1655*, 13–28.
(10) Cukier, R. I.; Nocera, D. G. *Annu. Rev. Phys. Chem.* **1998**, *49*, 337–369.
(11) Trasatti, S. In *Electrochemistry of Novel Materials*; Lipkowski, J., Ross, P. N., Eds.; VCH: New York, 1994; Ch. 5.
(12) Tarasevich, M. R.; Efremov, B. N. In *Electrodes of Conductive Metal Oxides, Part A*; Trasatti, S., Ed.; Elsevier: Amsterdam, 1980; Ch. 5.
(13) Miles, M. H.; Klaus, E. A.; Gunn, B. P.; Locker, J. R.; Serafin, W. E.; Srinivasan, S. *Electrochim. Acta* **1978**, *23*, 521–526.
(14) Matsumoto, Y.; Sato, E. *Mater. Chem. Phys.* **1986**, *14*, 397–426.
(15) Hoare, J. P. *The Electrochemistry of Oxygen*; Interscience: New York, 1968.

oxidation is thought to precede a turnover-limiting electrochemical step involving the removal of one proton and one electron to form a surface oxide species (Scheme 1).[17−20] The shift in mechanism between the pH extremes has been attributed to the kinetic facility of oxidizing hydroxide ion relative to water.[21] As such, studies of the OER on platinum oxides establish the importance of evaluating electrode kinetics across a wide pH range.

In contrast to precious metal oxides, first-row transition metal spinels and perovskites have been studied mechanistically under only alkaline conditions[22−31] because oxide dissolution accompanies O_2 evolution under acidic conditions.[21] Even under alkaline conditions, a mechanistic consensus has been elusive because the identity of the substrate, method of preparation, and thickness of the oxide layer strongly impact the current−voltage characteristics and the observed reaction order with respect to hydroxide. The variability in kinetic data may be ascribed, in large part, to a barrier to electron transfer imposed by the oxide film. These barriers may be of an ohmic or nonohmic nature and serve to obscure the kinetics of the interfacial reaction chemistry.[20,30,32−36]

While some of these precious and nonprecious metal oxides have been optimized for use in commercial electrolyzers,[37] these technologies remain expensive for nonconcentrated solar energy storage applications.[38] As such, we have turned our attention to developing inexpensive, highly manufacturable, water-splitting catalysts for nonconcentrated solar energy storage. We have recently described the self-assembly of a highly active cobalt-based oxygen evolving catalyst that forms as a thin film on inert electrodes when aqueous solutions of Co^{2+} salts are electrolyzed in the presence of phosphate (Co-Pi) or borate (Co-Bi);[39,40] more recently, we have used a similar strategy to discover a Ni-Bi catalyst.[41] These catalysts are of interest because they: (1) form in situ under mild conditions on a variety of conductive substrates;[39−41] (2) exhibit high activity in pH 7−9 water at room temperature;[39,40] (3) are functional in salt water;[40] (4) are comprised of inexpensive, earth-abundant materials;[39,40] (5) self-heal by reversing catalyst corrosion at open circuit upon application of a potential;[42] (6) can be interfaced with light absorbing and charge separating materials to effect photoelectrochemical water splitting;[43−45] and (7) are functional models of the oxygen-evolving complex of Photosystem II.[46] The simple operation of the catalyst from conventional water sources under benign conditions is an important step toward providing distributed solar energy storage at low-cost.[47]

The further development of new catalysts for water splitting will benefit from an understanding of the OER process of Co-Pi. EXAFS studies support a structural model wherein Co-Pi is composed of cobaltate clusters of molecular dimensions.[48] In addition, XANES[48] and EPR[49] studies are consistent with a proportion of cobalt centers attaining an oxidation state of IV during water oxidation catalysis. Against this backdrop, we now report the electrochemical kinetics and ^{18}O isotope studies of the OER catalyzed by Co-Pi in neutral water. The ability to perform electrokinetic studies of an amorphous thin film consisting of cobaltate clusters circumvents the difficulties imposed by electron transport barriers in interpreting the electrokinetics of the aforementioned metal oxide catalysts. Controlled low potential deposition of ultrathin catalyst films (∼60−600 nmol Co/cm^2) enables the kinetics of water oxidation chemistry to be isolated. As such, the current−voltage behavior of Co-Pi and measurements of the relevant reaction orders reveal a viable mechanism for the OER at neutral pH that is consistent with spectroscopic and structural studies of the catalyst.

Results

Catalyst films were grown by controlled potential electrolysis of 0.5 mM Co^{2+} solutions in 0.1 M potassium phosphate electrolyte, pH 7.0 (Pi electrolyte). Performing the electrolysis at 1.3 V (vs NHE) gives rise to a catalyst film of several micrometer thickness after the course of several hours.[39,40]

(16) Appleby, A. J. In *Modern Aspects of Electrochemistry*; Bockris, J. O. M., Conway, B. E., Eds.; Plenum: New York, 1973; Vol. 9; p 369.
(17) Conway, B. E.; Liu, T. C. *Langmuir* **1990**, *6*, 268–276.
(18) Conway, B. E.; Liu, T. C. *Proc. Royal Soc. London, Ser. A* **1990**, *429*, 375–379.
(19) Birss, V. I.; Damjanovic, A. *J. Electrochem. Soc.* **1987**, *134*, 113–117.
(20) Birss, V. I.; Damjanovic, A.; Hudson, P. G. *J. Electrochem. Soc.* **1986**, *133*, 1621–1625.
(21) Conway, B. E.; Tilak, B. V. In *Advances in Catalysis*; Eley, D. D., Pines, H., Weisz, P. B., Eds.; Academic Press: New York, 1992; Vol. 38; pp 78−98.
(22) Bockris, J. O'M.; Otagawa, T. *J. Phys. Chem.* **1983**, *87*, 2960–2971.
(23) Willems, H.; Kobussen, A. G. C.; De Wit, J. H. W.; Broers, G. H. J. *J. Electroanal. Chem.* **1984**, *170*, 227–242.
(24) Willems, H.; Kobussen, A. G. C.; De Wit, J. H. W.; Broers, G. H. J. *J. Electroanal. Chem.* **1985**, *194*, 287–303.
(25) Singh, S. P.; Samuel, S.; Tiwari, S. K.; Singh, R. N. *Int. J. Hydrogen Energy* **1996**, *21*, 171–178.
(26) Singh, R.-N.; Hamdani, M.; Koenig, J.-F.; Poillerat, G.; Gautier, J. L.; Chartier, P. *J. Appl. Electrochem.* **1990**, *20*, 442–446.
(27) Singh, R. N.; Koenig, J.-F.; Poillerat, G.; Chartier, P. *J. Electrochem. Soc.* **1990**, *137*, 1408–1413.
(28) Conway, B. E.; Liu, T. C. *Ber. Bunsen-Ges. Phys. Chem.* **1987**, *91*, 461–469.
(29) Castro, E. B.; Gervasi, C. A. *Int. J. Hydrogen Energy* **2000**, *25*, 1163–1170.
(30) Lyons, M. E. G.; Brandon, M. P. *Int. J. Electrochem. Sci.* **2008**, *3*, 1425–1462.
(31) Svegl, F.; Orel, B.; Grabec-Svegl, I.; Kaucic, V. *Electrochim. Acta* **2000**, *45*, 4359–4371.
(32) Damjanovic, A.; Jovanovic, B. *J. Electrochem. Soc.* **1976**, *123*, 374–381.
(33) Meyer, R. E. *J. Electrochem. Soc.* **1960**, *107*, 847–853.
(34) MacDonald, J. J.; Conway, B. E. *Proc. Royal Soc. London, Ser. A* **1962**, *269*, 419–440.
(35) Soderberg, J. N.; Co, A. C.; Sirk, A. H. C.; Birss, V. I. *J. Phys. Chem. B* **2006**, *110*, 10401–10410.
(36) Banham, D. W.; Soderberg, J. N.; Birss, V. I. *J. Phys. Chem. C* **2009**, *113*, 10103–10111.
(37) Grimes, C. A.; Varghese, O. K.; Ranjan, S. *Light, Water, Hydrogen: The Solar Generation of Hydrogen by Water Photoelectrolysis*; Springer: New York, 2008.
(38) Turner, J. A. *Science* **1999**, *285*, 687–689.
(39) Kanan, M. W.; Nocera, D. G. *Science* **2008**, *321*, 1072–1075.
(40) Surendranath, Y.; Dincă, M.; Nocera, D. G. *J. Am. Chem. Soc.* **2009**, *131*, 2615–2620.
(41) Dincă, M.; Surendranath, Y.; Nocera, D. G. *Proc. Natl. Acad. Sci. U.S.A.* **2010**, *107*, 10337–10341.
(42) Lutterman, D. A.; Surendranath, Y.; Nocera, D. G. *J. Am. Chem. Soc.* **2009**, *131*, 3838–3839.
(43) Zhong, D. K.; Sun, J.; Inumaru, H.; Gamelin, D. R. *J. Am. Chem. Soc.* **2009**, *131*, 6086–6087.
(44) Zhong, D. K.; Gamelin, D. R. J. Am. Chem. Soc. **2009**, DOI: 10.1021/ja908730h.
(45) Steinmiller, E. M. P.; Choi, K. S. *Proc. Natl. Acad. Sci. U.S.A.* **2009**, *106*, 20633–20636.
(46) Kanan, M. W.; Surendranath, Y.; Nocera, D. G. *Chem. Soc. Rev.* **2009**, *38*, 109–114.
(47) Nocera, D. G. *ChemSusChem* **2009**, *2*, 387–390.
(48) Kanan, M. W.; Yano, J.; Surendranath, Y.; Dincă, M.; Yachandra, V. K.; Nocera, D. G. J. Am. Chem. Soc. **2010**, *132*, 13692−13701.
(49) McAlpin, J. G.; Surendranath, Y.; Dincă, M.; Stich, T. A.; Stoian, S. A.; Casey, W. H.; Nocera, D. G.; Britt, R. D. *J. Am. Chem. Soc.* **2010**, *132*, 6882–6883.

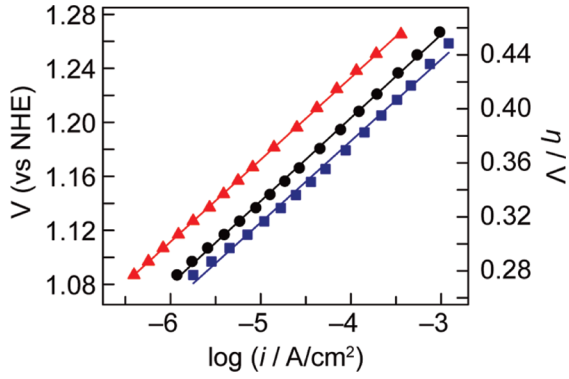

Figure 1. Tafel plots, $V = (V_{appl} - iR)$, $\eta = (V - E°)$, for catalyst films grown with passage of 6 (▲), 24 (●), and 60 (■) mC/cm^2.

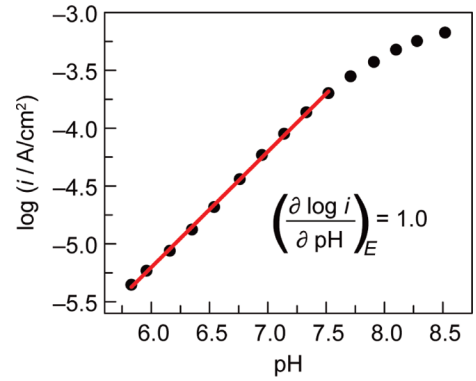

Figure 2. pH dependence of steady-state catalytic current density at constant potential ($E = 1.18$ V) for a catalyst film functioning in 0.1 M Pi electrolyte.

Whereas this procedure leads to rapid catalyst formation, the growth of the film is accompanied by significant O_2 evolution at this potential. As such, the charge passed in a deposition is not representative of the number of Co atoms deposited, making it difficult to produce films of reproducible thickness and catalyst loading. To avoid this problem, films used in the electrochemical studies here were prepared by controlled potential electrolysis at 1.05 V. As determined by independent measurements of catalyst films in Co^{2+}-free Pi solution, negligible water oxidation catalysis occurs at this potential. Thus, the charge passed at 1.05 V during a deposition is a direct measure of Co^{2+} oxidation and therefore provides an upper limit for the number of Co ions incorporated into the film. Double layer charging currents can be neglected owing to the long duration of a typical deposition (~1 h).

The current−voltage (Tafel) behavior of the catalyst in the region of water oxidation was measured over a 210 mV range in 10 − 30 mV increments. Electrolysis was conducted at each potential in Co-free Pi electrolyte until the current density (i) reached a steady state value. The potential values were converted to overpotential values (η) by correcting for ohmic potential losses and subtracting the thermodynamic potential for water oxidation under the experimental conditions (see Supporting Information). Tafel data were collected using freshly prepared films that were deposited with passage of 6, 24, and 60 mC/cm^2 (Figure 1). Estimating that each Co atom, together with its surrounding ligands, occupies a volume of 125 Å^3 (see SI), these deposition currents correspond to approximate film thicknesses of 10, 40, and 90 nm, respectively. For catalysts prepared from the passage of 6 and 24 mC/cm^2, linearity in the Tafel plot (η vs log(i)) is observed over 3 orders of magnitude; a slight curvature is observed for the catalyst prepared with the passage of 60 mC/cm^2. The activity of the film increases monotonically as the catalyst loading and film thickness increase but the Tafel slope does not change appreciably; Tafel slopes of 61, 62, and 60 mV/decade are observed for 6, 24, and 60 mC/cm^2 depositions, respectively. These slopes for the three films of different thicknesses are near the 59 mV/decade value that corresponds to $2.3 \times RT/F$. This slope is characteristic of an O_2 evolution mechanism involving a reversible one-electron transfer prior to a chemical turnover-limiting step (vide infra).[50] The Tafel slopes are highly reproducible among independent and sequential runs (Figures S1 and S2 of the SI) and they are not dependent on the direction of potential scan (Figure S3), indicating that the films are not appreciably altered during Tafel data collection. Tafel plots were also measured for catalyst films deposited on a Pt disk electrode rotated at 1000 and 2000 rpm; the Tafel slopes (Figure S4) for these two different rotation rates were identical, indicating that the reaction is not subject to limitations of mass transport over the current range studied here.

Figure 1 also provides the lower limit of the turnover frequency for O_2 production per Co. In this work, films were prepared at a potential where oxygen evolution does not occur. Thus, the number of Co atoms deposited in the catalyst film is proportional to the charge passed (C) during film deposition with the assumption that deposition results from a Co^{II} to Co^{III} oxidation reaction. Such an assumption is validated by EPR[49] and XAS[48] studies, which point to a predominantly Co^{3+} containing film at the potential of electrodeposition, 1.05 V. Applying the equation, i/4C, yields a lower limit turnover frequency at $\eta = 410$ mV of 2.6, 2.0, and 1.4×10^{-3} s^{-1} for 6, 24, and 60 mC/cm^2 films, respectively.

The pH dependence of Co-Pi was examined by introducing the catalyst film into Co-free Pi electrolyte solutions. The potential applied to the catalyst was held constant at 1.18 V and the pH of the solution was incrementally increased from 5.8 − 8.5. The electrode was operated at each pH step for 5 min to ensure that the pH and current had attained steady state conditions. Measurement of the current density at fixed potential allows for the direct interrogation of the reaction order in H^+ activity. A plot of the log of the current density vs pH (Figure 2) exhibits linearity from pH 5.8−7.5 and a slope of 1.0 whereas a negative deviation from linearity is observed beyond pH 8. At pH values greatly exceeding the second pK_a (7.2) of phosphate, the electrolyte becomes a poor buffer and the local pH is suppressed relative to its bulk value, resulting in attenuated current densities. The problem is compounded by the fact that the current density is expected to increase in an exponential fashion as the pH is increased at constant applied potential, rapidly overwhelming the buffering capacity of phosphate.

To examine the pH dependence of water oxidation over a wider range of pH values, a galvanostatic titration was conducted. The potential required to sustain a constant current density of 30 μA/cm^2 was measured while the pH was incremented from 4.6 to 12 (Figure 3). At this low current density, local pH gradients are obviated and the potential varies linearly with pH up to ~9.2, after which a slight negative deviation in the slope is observed. A linear fit of the data in Figure 3 over the pH range 4.6 − 9.2 yields a slope of −64 mV/pH unit. The data are unaffected (Figure S5) by repeating

(50) Gileadi, E. *Electrode Kinetics for Chemists, Chemical Engineers, and Materials Scientists*; Wiley-VCH: New York, 1993; pp 127−184.

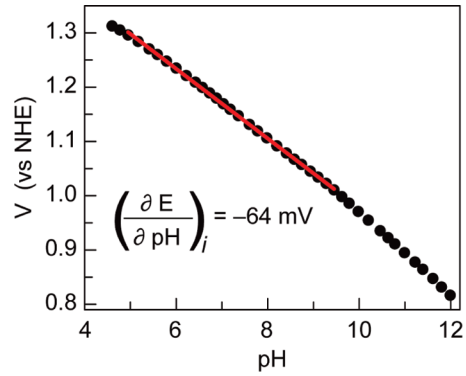

Figure 3. pH dependence of steady-state electrode potential at constant current density (i_{anodic} = 30 μA/cm^2) for a catalyst film operated in 0.1 M Pi electrolyte.

the titration in the presence of excess inert electrolyte, 0.5 M KNO_3, ruling out diffuse double layer effects.[51,52] In this galvanostatic experiment, the potential dependence of the current density (the Tafel behavior) is convoluted with the slope of the potential vs pH plot.[50] Specifically,

$$\left(\frac{\partial E}{\partial pH}\right)_i = -\left(\frac{\partial E}{\partial \log(i)}\right)_{pH}\left(\frac{\partial \log(i)}{\partial pH}\right)_E \quad (1)$$

Thus, the observed −64 mV/pH unit slope in the galvanostatic experiment is consistent with the Tafel slope of 62 mV/decade obtained from potentiostatic measurements for unity order in pH, as observed in Figure 2. These studies establish a first order dependence of log(i) on pH and, therefore, an inverse first order dependence of the current density on proton activity.

The dependence of the current density on the concentration of phosphate in solution was ascertained from Tafel data that were collected on catalyst films operating in Pi electrolyte solutions at concentrations of [Pi] = 0.03, 0.1, 0.3, and 1 M at pH 7.0 (Figure S6). In the case of 0.03 M Pi electrolyte, 0.07 M $NaClO_4$ was added to maintain solution conductivity. Tafel data were collected from independently prepared films from depositions that passed 24 mC/cm^2. All Tafel plots exhibit slopes between 60 and 62 mV/decade and exchange current densities between 4 and 6 × 10^{-11} A/cm^2 (Figure S6). Interpolation of each Tafel plot at 1.10, 1.15, 1.20, and 1.25 V yields steady state current data as a function of the log of the phosphate concentration (Figure 4). Consistent with the similarity in Tafel slopes and exchange current densities, a zeroth order dependence on phosphate concentration is observed at each potential.

The kinetic profile of the catalyst in the absence of a proton-accepting electrolyte was determined by interrogating catalyst performance in $NaClO_4$ solutions. Steady state current densities were measured on a 24 mC/cm^2 catalyst film deposited on a Pt rotating disk electrode in 0.1 M $NaClO_4$ at pH 8 for a variety of rotation rates, ω, and applied potentials. The bulk pH was maintained at 8.00 ± 0.05 over the duration of the experiment by periodic addition of dilute NaOH (see SI). For each potential value examined, a Koutecký-Levich plot of i^{-1} vs $\omega^{-1/2}$ (Figure S7) was extrapolated to infinitely high rotation rate ($\omega^{-1/2} = 0$) to determine the activation controlled current density in the absence of mass-transport limitations.[53] For all data points, ohmic potential losses amounted to less than 1 mV and were ignored. Figure 5 shows the Tafel plot of the applied potential vs the log of the activation controlled current density. The data points exhibit linearity over a 0.15 V potential range and a slope of 170 mV/decade. Upon collection of Tafel data in 0.1 M $NaClO_4$, the Tafel plots of the same films were recorded in 0.1 M Pi electrolyte at pH 8.0. Tafel slopes of 59 mV/decade were obtained, similar to that observed at pH 7.

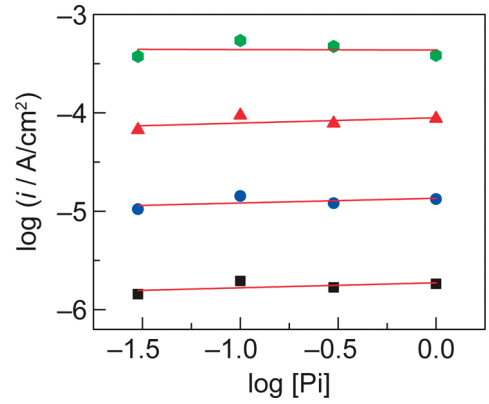

Figure 4. Phosphate concentration dependence of steady-state catalytic current density at constant potential (E = 1.10 V (■), 1.15 V (●), 1.20 V (▲), 1.25 V (⬢)) for a catalyst film operated in Pi electrolyte. For all potentials, the order in phosphate is effectively zero.

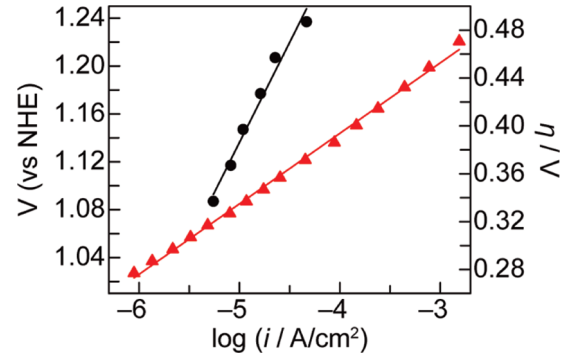

Figure 5. Tafel plots, $V = (V_{appl})$, $\eta = (V - E°)$, of Co-Pi catalyst films deposited on Pt rotating disk electrodes and operated in cobalt-free 0.1 M $NaClO_4$, pH 8.0 (●). Activation controlled current density values were derived from Koutecký-Levich analysis of steady-state current densities measured at multiple rotation rates. Data are the average of three independent runs and error limits fall within the size of the points. The Tafel plot (▲) of a catalyst film evaluated at 2000 rpm rotation rate in 0.1 Pi electrolyte pH 8.0 immediately after data collection in 0.1 M $NaClO_4$ is shown for comparison. Tafel slopes are 170 (●), and 59 (▲) mV/decade.

Cyclic voltammetry (CV) of a 24 mC/cm^2 catalyst film in Co-free Pi electrolyte was employed to examine oxidation state changes in the film as a function of applied potential (Figure 6). On the initial anodic sweep from the resting potential, a featureless rise in current is observed through the catalytic wave. The return cathodic scan exhibits two very broad peaks at 1.10 and 0.87 V, both of which become more ill-defined upon further scanning. Subsequent anodic scans exhibit a very broad anodic wave with a half-wave potential of 0.92 V followed by onset of catalysis at ~1.1 V. Integration of the anodic feature prior to 1.09 V accounts for 20% of the Co that was deposited in the film. All of the CV features are preserved after the electrode

(51) Parsons, R. In *Advances in Electrochemistry and Electrochemical Engineering*; Delahay, P., Tobias, C. W., Eds.; Interscience: New York, 1961; Vol. 1, pp 29−64.
(52) Angelinetta, C.; Falciola, M.; Trasatti, S. *J. Electroanal. Chem.* **1986**, *205*, 347–353.
(53) Bard, A. J.; Faulkner, L. R. *Electrochemical Methods: Fundamentals and Applications*; Wiley; New York, 2001; pp 340−344.

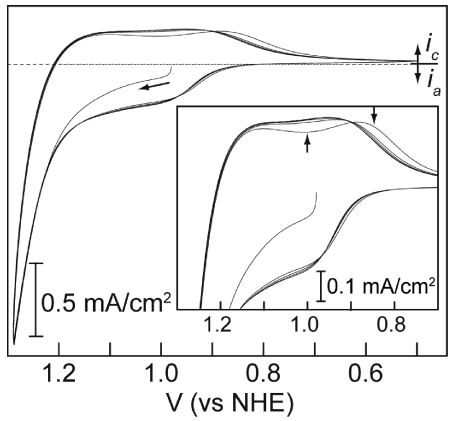

Figure 6. Cyclic voltammogram of a freshly prepared catalyst-coated FTO electrode, 10 mV/s scan rate, in 0.1 M Pi electrolyte, pH 7.0. Background trace of an uncoated FTO electrode in the same electrolyte medium (- - -). Five consecutive cycles, taken without pause, are shown. Up and down arrows indicate progression upon successive scanning.

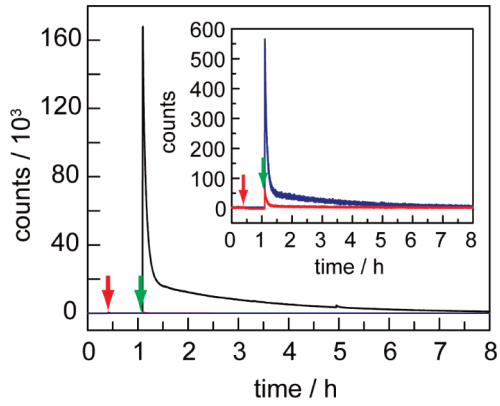

Figure 7. In-line MS detection of evolved $^{32}O_2$ (black line), $^{34}O_2$ (blue line), and $^{36}O_2$ (red line) from a catalyst film enriched with 87% ^{18}O and operated in unenriched 0.1 M Pi electrolyte solution. Film prepared in a deposition that passed 30 mC (4.2 mC/cm^2). The cell was isolated from the MS (red arrow), operated galvanostatically at 6 mA (0.83 mA/cm^2) for 27.8 min (10 C passed), allowed to equilibrate, and reopened (green arrow) to the MS. Inset shows $^{34}O_2$ (blue line), and $^{36}O_2$ (red line) signals on an expanded ordinate axis.

has been subjected to two consecutive collections of Tafel data, indicating that the electrode is not significantly altered over the course of Tafel data collection. Repetitive scanning over the range 0.5 − 1.25 V leads to minimal diminishment in the anodic and cathodic waves and the magnitude of the catalytic wave is unaltered. No additional cathodic features are observed if the return scans are extended to 0.0 V.

Insight into the nature of the O−O bond formation step is furnished from measurements of the isotopic distributions of O_2 evolved from ^{18}O-enriched catalyst films operating in nonenriched Pi electrolyte. The ^{18}O-enriched catalyst films were prepared by controlled potential electrolysis of 0.5 mM Co^{II} in Pi electrolyte solutions enriched with 87% $^{18}OH_2$. Electrodepositions of the catalyst films were carried out at 1.10 V with the passage of 1.5−6.8 mC/cm^2. At this voltage, the film forms but does not evolve oxygen. The amounts of charge passed in the depositions correspond to film thicknesses of ≤10 nm (vide supra). The use of extremely thin films minimized the amount of $^{18}OH_2$ that could be trapped in the film. Following the deposition from a Co^{II} solution in 87% $^{18}OH_2$, the electrodes with the catalyst films were transferred to Co^{II}-free Pi electrolyte enriched with 87% $^{18}OH_2$, pulsed at 1.3 V for 100 s to effect catalytic turnover in the enriched electrolyte, and then allowed to equilibrate at open circuit for 30 min. Films were then thoroughly rinsed in nonenriched Pi electrolyte (natural abundance of $^{18}O = 0.2\%$) and placed in a gastight electrochemical cell containing nonenriched Pi electrolyte that was placed in-line with a mass spectrometer (MS). The cell was purged of atmospheric O_2 until the signal reached a baseline level (data shown in Figure 7 prior to the red arrow). The cell was then isolated from the MS and electrolysis was initiated (data shown in Figure 7 after the red arrow). Upon conclusion of electrolysis, the cell was opened to the MS (data shown after green arrow in Figure 7). The signals for $^{32}O_2$, $^{34}O_2$ and $^{36}O_2$ rise rapidly, reach a peak after several minutes, and decay back to their baseline levels over the course of 6−8 h. In certain cases, the experiment was repeated using the same electrochemical cell and electrode after all MS signals had returned to their baseline levels. All traces were corrected for the instrument background for each signal, as well as residual air. In addition, the $^{34}O_2$ signal was corrected for $^{34}O_2$ produced statistically from the 0.2% $^{18}OH_2$ present in nonenriched water. This residual $^{18}OH_2$ contributed negligibly to the $^{36}O_2$ signal and was ignored. We also note that if exchange of the ^{18}O label in the catalyst film with bulk solvent was complete, it would contribute $<2 \times 10^{-5}$ % to the 0.2% natural abundance of $^{18}OH_2$ in nonenriched solution and accordingly any contribution to $^{34}O_2$ produced statistically from such exchange was ignored.

Table 1. Ratio of $^{32}O_2$ to $^{34}O_2$ Released from 87% ^{18}O-Enriched Catalyst Films

no.	deposition[a]	electrolysis[b]	$^{32}O_2/^{34}O_2$	% ^{18}O extruded
1	10 mC (1.5 mC/cm^2)	0.55 C (0.08 C/cm^2)	120	7
2	30 mC (4.9 mC/cm^2)	1.4 C (0.23 C/cm^2)	140	5
3a[c]	30 mC (6.8 mC/cm^2)	1.4 C (0.32 C/cm^2)	110	6
3b[c]		1.4 C (0.32 C/cm^2)	140	5
4a[c]	30 mC (4.2 mC/cm^2)	10.0 C (1.4 C/cm^2)	310	15
4b[c]		10.0 C (1.4 C/cm^2)	710	7

[a] Charge passed during electrodeposition in 87% ^{18}O-enriched Pi electrolyte. [b] Charge passed during electrolysis in unenriched Pi electrolyte immediately prior to MS detection. [c] Letters a and b denote first and second electrolysis runs using the same electrode.

Table 1 summarizes the results of the labeling experiments. The charge passed during the deposition in ^{18}O-enriched electrolyte was varied from 1.5 to 6.8 mC/cm^2 while the charge passed during electrolysis in nonenriched Pi electrolyte was varied from 0.55 to 10.0 C. Noting that oxygen evolution occurs with quantitative Faradaic efficiency,[39,40] the total charge passed in each electrolysis was used to determine the moles of O_2 evolved. Integration of the $^{32}O_2$ and $^{34}O_2$ peaks was used to estimate the ratio of the amounts of the two gases evolved in each run and this ratio, combined with the moles of O_2 evolved, was used to estimate the percentage of the deposited ^{18}O label that was extruded from the material as $^{34}O_2$ during electrolysis in nonenriched electrolyte.

Isotopic distributions of O_2 evolved from $^{18}OH_2$-enriched catalyst films indicate that a significant percentage of the estimated total ^{18}O contained in the films was extruded in the form of $^{34}O_2$ and, to a lesser extent, $^{36}O_2$ (Table 1 and SI). The extrusion of the label did not occur in an initial burst of $^{34}O_2$ or $^{36}O_2$ from the film, as indicated by isotopic distributions recorded after very short electrolyses (data not shown). Thus, appreciable ^{18}O extrusion that enabled MS detection of $^{34}O_2$ and $^{36}O_2$ required prolonged electrolyses. Consequently, the MS counts consist of considerably more $^{32}O_2$ than $^{34}O_2$ or $^{36}O_2$. For

electrolyses that passed 0.55 − 1.4 C, (0.08 − 0.32 C/cm^2), the ratio of $^{32}O_2$ to $^{34}O_2$ was greater than 100:1. Electrolyses that passed significantly larger amounts of charge (10 C, 1.4 C/cm^2), exhibited ratios of ∼300 − 700:1. Subsequent electrolyses after MS signals returned to baseline levels utilizing the same electrode exhibited additional ^{18}O extrusion. Together, the results indicate a progressive extrusion of ^{18}O in the form of $^{34}O_2$ or $^{36}O_2$ from the enriched catalyst concomitant with the catalytic production of a large excess of $^{32}O_2$. Extensive electrolysis (passage of 20 C) of a catalyst film (30 mC deposition) over two consecutive runs led to an aggregate extrusion of 22% of the ^{18}O label (runs 4a and 4b in Table 1) after 12 h.

Discussion

The Tafel relation between potential and the steady state current density together with studies of the reaction order with respect to pH provide a basis for mechanistic interpretation of the OER catalyzed by Co-Pi. The current density measured at steady state is directly proportional to the rate of the underlying reaction for electrochemical reactions that are not mass-transport limited.[50] This condition applies to the electrokinetic studies of Co-Pi described here, as evidenced by the rotating disk current−voltage data shown in Figure S4. Tafel plots collected at 1000 and 2000 rpm of Co-Pi films on a Pt rotating disk electrode exhibit similar slopes (61 mV/decade) to those collected on a stationary FTO electrode (62 mV/decade) in a stirred solution, indicating that the observed currents are not limited by mass transport to the catalyst films over this current/potential range (Figure S4). The Tafel data is reproducible between sequential potential sweeps (Figure S1) and is insensitive to the direction of potential sweep (Figure S3), indicating that the film is not appreciably altered over the course of Tafel data collection. In addition, measurable steady-state current is observed upon application of an overpotential of >0.2 V. At these overpotentials, any current arising from the oxygen reduction back reaction can be safely ignored and, thus, kinetic information about the OER can be deduced directly from the steady state current (rate) measurements.

Although the activity of the film increases markedly as the film thickness is increased from 10 to 90 nm, the slope of the Tafel plot is similar over the same range of current densities for all thicknesses examined, indicating that the reaction kinetics are not influenced by barriers to electron transport or mass transport within the film (Figure 1). We note that the films examined in this study are significantly thinner than the ∼1 μm thick films reported originally.[39,40] Tafel plots of those films exhibit higher slopes and slight deviations from linearity at high current densities, suggesting that barriers to electron and/or mass transport within the film do arise for thick catalyst layers. The Tafel slope of nearly 59 mV/decade observed for the thin films studied here indicates that a single mechanism is dominant over the potential range investigated. The transfer coefficient for the OER is 1, which is consistent with a chemical turnover limiting step following a single electron pre-equilibrium (vide infra).[50] Inasmuch as the electrochemical kinetics are not sensitive to film thickness for films <100 nm, increased activity with increasing thickness of the film is likely due to an increased number of active sites and not due to an increase in the intrinsic rate of turnover of those active sites. Indeed, all three film thicknesses exhibit similar lower limit turnover frequencies (TOF) of ∼2 × 10^{-3} s^{-1} at an overpotential of 410 mV. This TOF estimate assumes that every Co center in the film is catalytically active. Since the vast majority of the cobalt centers in the film are expected to play a purely structural role, this is a gross underestimate of the real TOF of active sites. However, as we currently have no direct measure of the electrocatalytically active surface area or the active site density, we present this value purely for the purposes of comparing different film thicknesses. The similarity in the TOF among films of varying thicknesses suggests that the films are permeable to the water substrate and that the OER is not confined to the outer surface of the catalyst layer. As such, higher geometric current densities for Co-Pi may be achieved simply by increasing the number of Co active sites on the anode by growing a thicker film. We note that the lower limit for the turnover frequency per Co atom of Co-Pi is similar to or exceeds most Co based water oxidation catalysts. For instance, turnover frequencies of 1140 s^{-1} have been reported for silica-templated nanoclusters of Co_3O_4 measured under photochemical conditions.[54] When one considers the number of Co atoms in the nanorods, a turnover frequency of ∼8 × 10^{-4} s^{-1} per Co of the entire nanoocluster, which is stated to be poorly crystalline, is similar to that of the Co-Pi system. We also note that the potential corresponding to the $[Ru(bpy)_3]^{2+}/S_2O_8^{2-}$ system used in the study of Co_3O_4 nanoclusters is difficult to define without knowing the details of the catalytic mechanism.

The OER involves the removal of four protons per equivalent of O_2 generated and thus an explicit pH dependence may be expected in the rate law for catalysis. Interrogation of the pH dependence by both potentiostatic (Figure 2) and galvanostatic (Figure 3) techniques indicates an inverse first-order dependence on proton activity, which is consistent with loss of a single proton in an equilibrium step prior to the turnover-limiting process. While phosphate is neither a reactant nor product in the overall water oxidation reaction, it can serve as a proton acceptor in reactions involving PCET transformations (vide infra).[55] Notwithstanding, the zeroth order dependence of phosphate over a >1.5 decade range of phosphate concentration (Figures 4 and S6) indicates that proton transfer to phosphate is not involved in the turnover-limiting step and therefore proton transfer is also not turnover-limiting since phosphate is the only viable proton acceptor in solution. Moreover, turnover-limiting proton transfer to surface bound phosphate is unlikely provided that phosphate has not saturated the catalyst film over the potential range studied here. We note that turnover-limiting internal proton transfers, as might be required for oxo-hydroxo exchange between catalyst active sites, cannot be ruled out.

The data in Figures 1−4 point to an electrochemical rate law that is described by the following expression:

$$i = k_0(a_{H^+})^{-1} \exp\left[\frac{FE}{RT}\right] \quad (2)$$

where k_0 is a potential-independent constant. This constant is proportional to the exchange current density and therefore will increase as catalyst loading increases as observed in Figure 1. The rate expression carries the observed inverse first order dependence on proton activity, $a_H{}^+$ (Figures 2 and 3), the zeroth order dependence on phosphate (Figure 4) and the exponential relationship with potential, E (Figure 1). Rearrangement of the log form of eq 2 yields a Tafel slope, $\partial E/\partial \log(i)$, of 59 mV/decade that is also consistent with the experimental data shown in Figure 1.

(54) Jiao, F.; Frei, H. *Angew. Chem., Int. Ed.* **2009**, *48*, 1841–1844.
(55) Irebo, T.; Reece, S. Y.; Sjödin, M.; Nocera, D. G.; Hammarström, L. *J. Am. Chem. Soc.* **2007**, *129*, 15462–15464.

Equation 2 is consistent with a mechanistic sequence involving a reversible one electron, one proton equilibrium step followed by a rate-limiting chemical step:[50]

$$A \rightleftharpoons B + e^- + H^+ \quad (3)$$

$$B \rightarrow C \quad (4)$$

For such a sequence, the reaction velocity at steady state, v, can be described by the following:[50]

$$v = k_2\theta_B \quad (5)$$

where k_2 is the rate constant for the chemical step (eq 4) and the θ_B is the surface coverage of the intermediate participating in the rate-limiting chemical transformation. Specifically, θ_B is the surface concentration of B (Γ, in mol/cm^2) divided by the maximum surface concentration (Γ_{max}). We note that the number of active sites in the film may represent a small proportion of the total number of solvent exposed Co centers in the film. Thus, Γ_{max} does not equal the number of exposed Co centers per cm^2, but rather the number of *active sites* per cm^2 and θ_B represents the fraction of these active sites in the form of intermediate B. Similarly, θ_A is the fraction of active sites in the form of intermediate A. The ratio of θ_B to θ_A is described by the Nernst equation,[50]

$$\frac{\theta_B}{\theta_A} = K_1(a_{H^+})^{-1}\exp\left[\frac{FE}{RT}\right] \quad (6)$$

where K_1 is the equilibrium constant at $E = 0$. This expression corresponds to a quasi-equilibrium assumption for the conversion of A to B (eq 3). Substituting for θ_B in eq 5 yields

$$v = \theta_A K_1 k_2 (a_{H^+})^{-1}\exp\left[\frac{FE}{RT}\right] \quad (7)$$

If the surface coverage of the catalyst in its resting state, A, is assumed to be appreciable (>0.9) throughout the potential range in which Tafel and other kinetic data are collected, then θ_A should not change appreciably with potential and, therefore, can be set to be constant. Under these conditions, eq 7 approximates the experimental rate law with

$$k_0 = 4F \times \theta_A \times K_1 k_2 \quad (8)$$

The assignment of chemical species to A, B, and C in reactions 3 and 4 is aided by insight into oxidation state changes in the film as a function of the applied potential. The CV of a freshly prepared catalyst film exhibits an anodic feature with a half-wave potential of 0.92 V and a very broad feature on the cathodic sweep that begins to decay at 0.9 V (Figure 6). No additional cathodic features are observed in CV scans taken to 0.0 V. The observed half-wave potential of 0.92 V is typical of a $Co^{II/III}$ redox couple; the $Co(OH)_2^{+/0}$ couple is estimated to be 1.1 V[56] and the Pourbaix diagram of cobalt indicates that oxidation of Co_3O_4 to Co(O)OH occurs at ~0.75 V at pH 7.[57] The $Co^{II/III}$ couple at 0.92 V for Co-Pi occurs ~0.17 V negative of the catalytic wave for water oxidation. Thus, the predominant Co oxidation state is expected to be III or higher during catalysis. Accordingly, we attribute the pre-equilibrium step (A $\rightleftharpoons$ B) to a formal $Co^{III} \rightleftharpoons Co^{IV}$ redox transition that is coupled to a proton transfer. The electrokinetic behavior described by eq 7 is in accord with Co^{IV} (B) as the minor component of this pre-equilibrium. As has been detailed in the literature,[50] θ_B must be less than 10% for the equilibrium to exhibit a Nernstian dependence on potential. Thus, at the highest potential (1.27 V) that Tafel data were collected, the maximum fractional surface coverage of Co^{IV} ($\theta_{B,max}$) is 10%, and θ_B is expected to diminish by an order of magnitude per 60 mV decrease in potential.

EPR spectra of Co-Pi films subjected to prolonged electrolysis at 1.14 V, a value sufficient for water oxidation, exhibit a Co^{IV} signal estimated to arise from 3% of the cobalt centers in the film.[49] Noting the sizable dead time (25 min) between termination of electrolysis and freezing of the EPR sample, we expect the population of Co^{IV} in the film during electrolysis at 1.14 V to be significantly in excess of the residual 3% observed by EPR. In line with this contention, recent in situ X-ray absorption near-edge spectroscopy (XANES) data are consistent with an appreciable population of Co^{IV} when the films are held at potentials sufficient for water oxidation catalysis.[48] The large population of Co^{IV} observed by EPR and in situ XANES suggests, therefore, that the catalyst resting state, A, is comprised of $Co^{III/IV}$ mixed valence clusters. The pre-equilibrium redox process (A $\rightleftharpoons$ B) therefore corresponds to further oxidation of the $Co^{III/IV}$ mixed valence clusters preceding a turnover-limiting chemical process.

The catalytic intermediates most commonly invoked for the OER reaction are M−OH_2, M−OH, and M−O species. The pH titration data of Figure 3 helps in distinguishing these species. The nearly linear dependence of the slope in Figure 3 to a pH of 12 suggests that the reactant in the equilibrium step defined by reaction 3 has a pK_a in excess of 12. The Pourbaix diagram of cobalt estimates a pK_a for $Co^{III}(OH_2)_6$ of 1.2.[57] Additionally, potentiometric titration data for Co_3O_4 indicates a pH of zero charge (pH_z) of ~7.5.[11] The pH_z estimates the average of the first and second pK_a values of surface bound water[58] and, therefore, suggests a first pK_a lower than 7.5. Thus, the pK_a of Co^{III}−OH_2 species on the catalyst surface in Co-Pi is expected to be much less than 12. As such, the pH titration data argues against an equilibrium between Co^{III}−OH_2 and Co^{IV}−OH. Taken together with the CV data, these results suggest that reaction 3 is defined by the following PCET equilibrium at pH 7,

$$[Co^{III}-OH] \rightleftharpoons [Co^{IV}-O] + H^+ + e^- \quad (9)$$

where the reactant side of eq 9 highlights the Co^{III} species of mixed valence cluster (species A) and the product side of eq 9 highlights oxidation of the center (species B). Under these pH conditions, the proton acceptor is HPO_4^{2-}. We note that the oxidation state assignments may be poorly representative of electronic structure since the charge may be delocalized among the Co atoms comprising the active site.

The PCET reaction of eq 9 persists in quasi-equilibrium during turnover in the presence of phosphate electrolyte. The key role of phosphate in maintaining this equilibrium is demonstrated by the Tafel behavior of catalyst films evaluated in 0.1 M $NaClO_4$, pH 8.0 (Figure 5). A Tafel slope of ~170 mV/decade is observed in this unbuffered medium along with a significant diminution of catalyst activity relative to the same

(56) Brunschwig, B. S.; Chou, M. H.; Creutz, C.; Ghosh, P.; Sutin, N. *J. Am. Chem. Soc.* **1983**, *105*, 4832–4833.
(57) Chivot, J.; Mendoza, L.; Mansour, C.; Pauporte, T.; Cassir, M. *Corros. Sci.* **2008**, *50*, 62–69.
(58) Daghetti, A.; Lodi, G.; Trasatti, S. *Mater. Chem. Phys.* **1983**, *8*, 1–90.

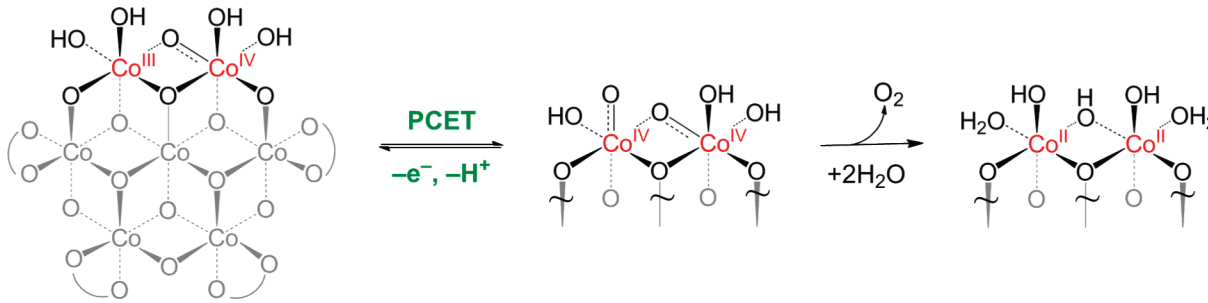

Figure 8. Proposed pathway for OER by Co-Pi. A PCET equilibrium proceeded by a turnover-limiting O−O bond forming step is consistent with current dependencies on proton and electron equivalencies. Curved lines denote phosphate, or OH_x terminal or bridging ligands.

film evaluated in Pi electrolyte at pH 8. The current densities plotted in Figure 5 are corrected for mass-transport limitations using Koutecký-Levich plots (Figure S7), and, thus, cannot be merely attributed to local pH changes. Tafel plots of a catalyst film in 0.1 M Pi, pH 8, generated immediately after experiments conducted in 0.1 M $NaClO_4$, pH 8.0, exhibit a slope of 59 mV/decade (Figure 5) and these Tafel data overlay with data obtained from a fresh film under identical conditions (Figure S8). This observation indicates that the film does not degrade during experiments in unbuffered solutions.

The marked increase in the Tafel slope in an unbuffered medium is consistent with a change in mechanism. Slopes significantly larger than 120 mV/decade are indicative of a turnover-limiting single electron transfer with a very high symmetry factor, β, which occurs from the catalyst resting state,[50] or a turnover-limiting chemical process occurring from the same resting state[22] (species A). In either case, the high slope indicates that the only available bases in an unbuffered medium (i.e., H_2O and ClO_4^-) cannot support the PCET equilibrium described in eq 9; at pH 8, the concentration of OH^- is too low to support this equilibrium. The inability of water to be an efficient acceptor in PCET reactions has also been observed in the PCET interconversions of homogeneous $Os^{II}-OH_2$, $Os^{III}-OH$, and $Os^{IV}=O$ complexes.[59] Studies of these osmium complexes and other systems have shown that buffers such as phosphate are efficient in triggering concerted PCET reactions that occur with high kinetic facility. These precedents, taken together with the results described here in unbuffered electrolyte, lead us to conclude that phosphate species, as opposed to OH_2 or OH^-, are the proton acceptors in the pre-equilibrium step. A buffer strength of 0.03 M is sufficient to maintain this equilibrium (Figure 4). While HPO_4^{2-} is the most efficient proton acceptor at pH 7, the linearity in the galvanostatic pH profile (Figure 3) to pH 4.6 suggests that $H_2PO_4^-$ is also a kinetically competent proton acceptor in this PCET equilibrium.

Films prepared from isotopically labeled $^{18}OH_2$-enriched water yield $^{32}O_2$ and $^{34}O_2$ and, to a lesser extent, $^{36}O_2$, when operated in nonisotopically labeled water (Figure 7). A real-time measure of the generation of labeled O_2 cannot be obtained because water oxidation must be performed over the time period of several minutes for appreciable quantities of O_2 to be detected by mass spectrometry (see SI). Additionally, to permit efficient purging of the in-line MS setup, ^{18}O-labeled catalyst films were equilibrated for a minimum of 1 h in unenriched water prior to electrolysis. Thus, interpretation of the results hinges on assumptions made regarding exchange of the label from catalyst films with bulk solvent. Rapid exchange of all or most of the label can be ruled out by the observation that substantial percentages of label are accounted for by $^{34}O_2$ and $^{36}O_2$. For example, over the course of two extensive electrolyses with the same film (passage of 2.8 C/cm^2 in aggregate, corresponding to >150 turnovers per Co), ~22% of the ^{18}O deposited in the material can be accounted for in $^{34}O_2$ and $^{36}O_2$ products. As noted above, the volume of the unenriched electrolyte used in these experiments is large enough that quantitative exchange of the labeled ^{18}O in the film with bulk solvent would contribute a negligible additional amount to the natural 0.2% ^{18}O abundance in the electrolyte. We note, however, that the extrusion of a substantial percentage of ^{18}O from the film in the form of $^{34}O_2$ and $^{36}O_2$ says little about the rate of exchange of ^{18}O atoms at active Co centers that may comprise a small portion of the material.

Labeling studies indicate that phosphate in a thick Co-Pi film exchanges appreciably with phosphate in solution in 1 h at both open circuit and at a potential sufficient for water oxidation.[42] These results suggest that terminal $Co-^{18}OH_x$ species in the extremely thin films used in the ^{18}O experiments here are subject to exchange with bulk solvent in the time required to purge the gastight electrochemical cell (>1 h) prior to the initiation of electrolysis. If the terminal $Co-^{18}OH_x$ species at active centers are exchanged with bulk solvent prior to electrolysis but μ-oxo/μ-hydroxide moieties at these centers are subject to much slower exchange, then the observation of $^{34}O_2$ and $^{36}O_2$ may be ascribed to the participation of μ-oxo/μ-hydroxide moieties in oxygen production. This proposal is in line with MS studies of $NiCo_2O_4$[60,61] and RuO_2[62] that demonstrate the participation of O-atoms of the oxide lattice in O_2 evolution. In this mechanistic picture, the slow extrusion of label during the catalysis may result from relatively slow migration of an ^{18}O to a position suitable for participation in O−O bond formation. Thus, multiple turnovers with μ-oxo/μ-hydroxide derived from unenriched solvent accompany a single turnover involving an ^{18}O originally incorporated in the film. We note, however, that this analysis assumes that a single mechanism predominates in the film. We cannot rule out that the slow extrusion of ^{18}O reflects a minor pathway for O_2 evolution that contributes negligibly to the observed electrokinetics. Due to the ambiguities associated with interpreting the ^{18}O-labeling results, studies that identify the rate and nature of oxo-exchange in these films are needed before specific conclusions can be drawn about the mechanism of O−O bond formation.

(59) Costentin, C.; Robert, M.; Savéant, J.-M.; Teillout, A.-L. *Proc. Natl. Acad. Sci. U.S.A.* **2009**, *106*, 11829–11836.
(60) Hibbert, D. B. *J. Chem. Soc., Chem. Commun.* **1980**, 202–203.
(61) Hibbert, D. B.; Churchill, C. R. *J. Chem. Soc., Faraday Trans. 1* **1984**, *80*, 1965–1975.
(62) Wohlfahrt-Mehrens, M.; Heitbaum, J. *J. Electroanal. Chem.* **1987**, *237*, 251–260.

A proposed reaction pathway for the overall transformation is shown in Figure 8 using the molecular cobaltate cluster model derived from XAS studies.[48] We note that catalytic active sites may reside on minority structural motifs in the film that are not observed by XAS. Given the pre-equilibrium shown in eq 3 and the observed 60 mV Tafel slope, the [$Co^{IV}-O$] product participates in a turnover-limiting chemical step. The electrochemical rate law is consistent with a proton independent chemical step and as such, it is reasonable to conclude that the O−O bond is formed in this irreversible chemical process. This turnover-limiting chemical process may be composed of one or more elementary chemical steps, which would be electrochemically indistinguishable. Mechanistic details of how the O−O bond forms and the precise nature of the turnover-limiting elementary step remain to be determined.

In summary, electrochemical studies show that O_2 production from Co-Pi involves a turnover-limiting chemical step that is preceded by a one-electron, one-proton PCET equilibrium step. The phosphate electrolyte plays the essential role of maintaining this PCET equilibrium by facilitating rapid proton transfer. Cyclic voltammetry experiments suggesting that the operative catalytic intermediate assumes a formal oxidation state of Co^{IV} and spectroscopic results point to a catalyst resting state composed of $Co^{III/IV}$ mixed valence clusters.

The kinetic observations made here inform future improvements to this catalyst system. Incorporation of metal atom dopants that lower the thermodynamic potential of the PCET pre-equilibrium or that promote a more facile O−O bond formation may lead to enhanced activity at lower overpotential. In cobaltate materials related to the catalysts reported here, transition metals such as Mn,[63] Ni,[64] and Ru[65] have been shown to substitute for Co. The effects of such metal ion substitution on the critical electrokinetic steps uncovered in this study are currently under investigation.

Acknowledgment. We thank M. Dincă for many productive discussions. This research was supported by the Center for Chemical Innovation of the National Science Foundation (CCI Powering the Planet, Grant Nos. CHE-0802907 and CHE-0947829), AFOSR FA9550-09-1-0689, and a grant from the Chesonis Family Foundation. Y.S. gratefully acknowledges the National Science Foundation for a predoctoral fellowship. M.W.K. gratefully acknowledges a Ruth Kirchstein NIH Postdoctoral Fellowship.

Supporting Information Available: Full experimental details, additional Tafel plots, and Koutecký-Levich plots. This information is available free of charge via the Internet at http://pubs.acs.org.

JA106102B

(63) Chen, Y -J.; Liu, C.-J.; Wang, J.-S.; Lin, J.-Y.; Sun, C. P.; Huang, S. W.; Lee, J. M.; Chen, J. M.; Lee, J. F.; Liu, D. G.; Yang, H. D. *Phys. Rev. B* **2007**, *76*, 092501/1−4.
(64) Gayathri, N.; Bharathi, A.; Sastry, V. S.; Sundar, C. S.; Hariharan, Y. *Sol. State Commun.* **2006**, *138*, 489–493.
(65) Strobel, P.; Muguerra, H.; Hebert, S.; Pachoud, E.; Colin, C.; Julien, M. *J. Sol. State Chem.* **2009**, *182*, 1872–1878.